



Ion-implanted silver nanoparticles for metal-enhanced fluorescence

Cite as: AIP Advances **8**, 095217 (2018); <https://doi.org/10.1063/1.5045570>

Submitted: 21 June 2018 . Accepted: 10 September 2018 . Published Online: 18 September 2018

Shahid Iqbal, Masoud Shabaninezhad , Mohammad Hatshan, Prashanta M. Niraula, Abubaker Abuhagr, Hasna Alali, Ramakrishna Guda, and Asghar Kayani 



View Online



Export Citation



CrossMark

ARTICLES YOU MAY BE INTERESTED IN

Gold nanoparticles ion implanted in glass with enhanced nonlinear optical properties

Journal of Applied Physics **75**, 3075 (1994); <https://doi.org/10.1063/1.356156>

Theoretical investigation of size, shape, and aspect ratio effect on the LSPR sensitivity of hollow-gold nanoshells

The Journal of Chemical Physics **150**, 144116 (2019); <https://doi.org/10.1063/1.5090885>

Ion beam modification of two-dimensional materials: Characterization, properties, and applications

Applied Physics Reviews **4**, 011103 (2017); <https://doi.org/10.1063/1.4977087>




NEW



AVS Quantum Science

A new interdisciplinary home for impactful quantum science research and reviews

Co-Published by

NOW ONLINE

Ion-implanted silver nanoparticles for metal-enhanced fluorescence

Shahid Iqbal,¹ Masoud Shabaninezhad,¹ Mohammad Hatshan,²
 Prashanta M. Niraula,¹ Abubaker Abuhagr,² Hasna Alali,¹
 Ramakrishna Guda,² and Asghar Kayani^{1,a}

¹*Department of Physics, Western Michigan University, Kalamazoo, Michigan 49008, USA*

²*Department of Chemistry, Western Michigan University, Kalamazoo, Michigan 49008, USA*

(Received 21 June 2018; accepted 10 September 2018; published online 18 September 2018)

Metal Enhanced Fluorescence (MEF) has promising applications in the field of optical displays, bio-sensing and photodynamic therapy. In this work, we exploit the plasmons of embedded silver nanoparticles (Ag NPs) fabricated by ion implantation to enhance the fluorescence of Coumarin515 dye (C515) via MEF. Ion Implantation of 70 keV Ag ions in quartz matrix at different fluences was carried out to synthesize Ag nanoparticles inside quartz matrix. The formation of Ag NPs is characterized by the optical absorption measurements and approximate sizes of Ag NPs was obtained from the fitting of the optical absorption spectra with Mie theory calculations. Rutherford Backscattering Spectrometry (RBS) measurement was used to obtain the depth profile and concentration Ag within the substrate. From the RBS results, it was determined that front edge of the layer containing Ag was formed at an average depth of 16 nm below the surface, which closely agreed with Stopping and Range of Ions in Matter (SRIM) calculations. Increase in the size of the NPs is observed as the fluence of the Ag within the substrate is increased. The MEF of drop casted C515 dye was studied using steady-state emission and excitation spectra measurements. Fluorescence enhancement factor ranging from 1.0 to 2.1 with a maximum enhancement for the largest size NP was obtained. The observed MEF was ascribed to a combination of plasmon enhancement with larger nanoparticles and to increased plasmonic hot spots. © 2018 Author(s). All article content, except where otherwise noted, is licensed under a Creative Commons Attribution (CC BY) license (<http://creativecommons.org/licenses/by/4.0/>). <https://doi.org/10.1063/1.5045570>

Plasmonic enhancement of optical properties has been a topic of intense investigations for several decades with Surface Enhanced Raman Scattering (SERS) being the driving force. SERS enhancement reaching as high as 10^{11} was observed that was attributed to combination of electromagnetic field as well as chemical enhancement.^{1–3} Another interesting aspect of plasmon enhancement is Metal Enhanced Fluorescence (MEF).^{4,5} MEF is the interaction of localized surface plasmons of metal nanoparticles (MNPs) and the excited state of fluorophore that amplifies the radiative quantum yield, resulting in enhancement of the fluorescence.⁶ MEF opens a path way for numerous applications in many areas of biotechnology and biomedical sciences⁷ such as bio-sensing,⁴ photodynamic therapy⁸ and imaging.⁵ MEF was successfully used for the detection of small protein⁹ and been studied in the context of LEDs¹⁰ and photonic crystal lasers.¹¹ MEF strongly depends upon the size, shape and the distance between the MNPs and fluorophore.^{6,12,13} Furthermore, plasmonic hotspots significantly contributes to MEF because of the intense field distribution between MNPs.^{14,15}

Several approaches were used to enhance fluorescence of fluorophore in the presence MNPs. Among all nanoparticles, Ag nanoparticles attracted significant research attention due to their unique physical and chemical properties such as good electrical conductivity, catalytic activity and Localized

^aCorresponding author's email address: asghar.kayani@wmich.edu

Surface Plasmon Resonance³ (LSPR). Zhang *et al.* achieved 2 to 3-fold fluorescence enhancement of fluorophores bound to cell membranes by using silver nano islands on glass substrate.¹⁶ Jang *et al.* used Ag particle monomer and Ag particle dimer with diameter of 20 nm and they obtained 7-fold and 13-fold single molecule Cyanine-5 fluorescence enhancement by placing it on the silver monomer and between silver particles dimer, respectively.¹⁷ In another work, Ag nano-triangles and silver nanorod arrays gave 16-fold and 50-fold fluorescence enhancement respectively in protein-immobilized indocyanine green¹⁸ dye on glass substrate.¹⁹

Most of the studies have been carried out using chemically synthesized MNPs.^{20,21} Problems with such an approach is the possibility of direct chemical interaction and also inability to properly control the distance between the nanoparticle and the fluorophore that results in quenching fluorescence.²¹ We synthesized metal nanoparticles of different sizes inside quartz matrices via ion implantation.²² This approach has three advantages, 1) it avoids direct interaction of fluorophore and nanoparticle, 2) the nanoparticles are formed without any surface capping agent, and 3) control is available on fluorophore and nanoparticle distance via the use of different energies of the ion beam.^{23,24} Ion implanted silver nanoparticles were studied previously.^{25,26} Benzo *et al.* have used ion implantation technique to synthesize embedded Ag NPs, Ag nanocrystals on SiO₂ target to study the aging of planes of silver nanoparticles²⁵ and near-field plasmonic effects on free surfaces.²⁶ Silver nanoparticles were formed in these matrices at different depths. Other reports of Ag NPs buried in different target matrixes were also reported.^{27,28,24,29–31} However, few reports were available wherein the embedded nanoparticles were used to study the plasmon enhancement effects.

In this study, various fluences of silver ions at 70 keV were utilized to tailor different size distribution of MNPs within the dielectric matrix. The PL enhancement of C515 dye in the presence of embedded Ag NPs was studied using combined steady-state and time-resolved fluorescence measurements. Fluorescence enhancement of C515 was successfully observed with respect to an increase in the silver concentration and sizes of silver nanoparticles.

Circular Fused quartz (SiO₂) of 99.99% purity, 1 mm thickness and 10 mm in diameter were ion implanted with 70 keV Ag⁻¹ ions at room temperature. Ion energy was selected by the Stopping and Range of Ions in Matter (SRIM)³² calculations. Negative ions were produced from a Source of Negative Ions by Cs Sputtering (SNICs II) connected to a Western Michigan University's (WMU) 6 MV Tandem Van De Graff Accelerator. Ag powder was used as a source cathode to extract negative ions to be bombarded on a substrate placed on LABVIEW controlled precision XY stage sample holder installed in low energy beam line of the WMU particle accelerator facility. Ion beam from the source was filtered and focused by a 20° dipole magnet and 50 kV einzel lens, respectively. Fluences of 0.8×10^{16} p/cm², 1.1×10^{16} p/cm², 1.3×10^{16} p/cm², 1.5×10^{16} p/cm² and 3.0×10^{16} p/cm², as obtained from Rutherford Backscattering Spectrometry (RBS) measurement, were used for this experiment. Collimator that defined the beam spot and the sample holder with the substrate were biased with the +50 V battery to trap secondary electrons within the material. Digital current integrator was used to measure total charge deposited on the sample holder. The total number of particles implanted was obtained from the total charge accumulated on sample divided by electronic charge.

To obtain the concentration and depth profile of implanted Ag in quartz, RBS was carried out with 2.5 MeV He⁺⁺ ions. Substrates surfaces were grounded to the sample holder to remove excess charge from the surface. Backscattered He particles were collected at an exit and scattering angles of 30° and 150° respectively using a surface barrier silicon detector.

To characterize Ag nanoparticles (NPs), absorption measurements were carried out using Shimadzu-UV-2101PC absorption spectrophotometer with 1 mm slit width. The simulation of optical absorption data to obtain the size of nanoparticles was carried out using Mie theory.³³ By comparing theoretical and experimental data, the average size and corresponding size distribution of the NPs in each sample was obtained.

For MEF studies, a stock solution of 100 μM C515 dye was prepared in ethanol and 40 μL was drop casted onto bare and Ag-implanted quartz substrates. Before drop casting, quartz surfaces were cleaned with acetone and dried by dry nitrogen. The steady state and time resolved fluorescence spectroscopy measurements were carried out using Edinburgh F900 spectrofluorometer. 450 W Xenon lamp was used as the excitation light source and R918 P was used as the

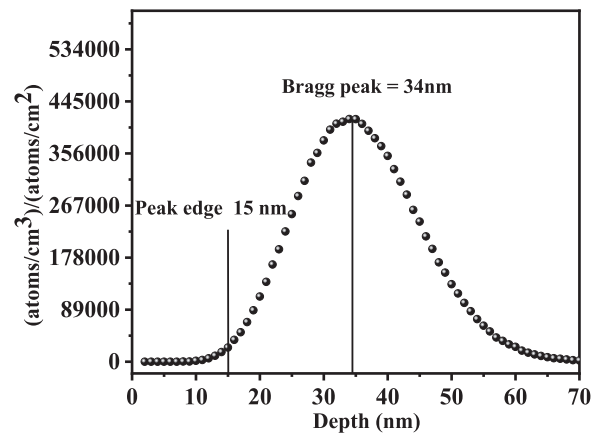


FIG. 1. SRIM simulations of 70 keV Ag ions in quartz substrate with Bragg peak and peak edge at 34 nm and 15 nm, respectively.

detector for steady-state fluorescence. The emission spectra of C515 were obtained by 350 nm and 450 nm wavelength. The excitation spectrum was measured keeping emission monochromator fixed at 510 nm. Slit widths for excitation and emission were fixed at 5 nm for all measurements. The measurements were repeated three times and error bars were obtained from such analysis. For fluorescence lifetime measurements, time-correlated single-photon counting measurements were carried out with 370 nm diode laser as excitation source with a repetition rate of 20 MHz. The decay traces were deconvoluted with instrument response function obtained using scatter.

Before the ion implantation of Ag in quartz, SRIM³² calculations were carried to obtain the depth distribution of 70 keV Ag-ions. A representative SRIM plot of 70 keV Ag⁺ ions in quartz is shown in the Fig. 1. The calculations were performed with 600,000 ions and the resultant plot gave Bragg-peak, which gives the maximum number of ions stopping at a certain depth, and the width which is due to energy straggling. The edge of the peak occurred at 15 nm, while the Bragg peak was at 34 nm, which means that maximum numbers of Ag ions are stopping at 34 nm below the surface. A representative RBS experimental and simulated plot of an Ag implanted substrate is presented in Fig. 2. The silicon and oxygen edges in the substrate were at 1457 keV and 960 keV whereas the implanted silver edge is at 2163 keV. Composition profiles for the as-implanted quartz substrates were generated using SIMNRA,³⁴ a computer simulation package for ion beam analysis.

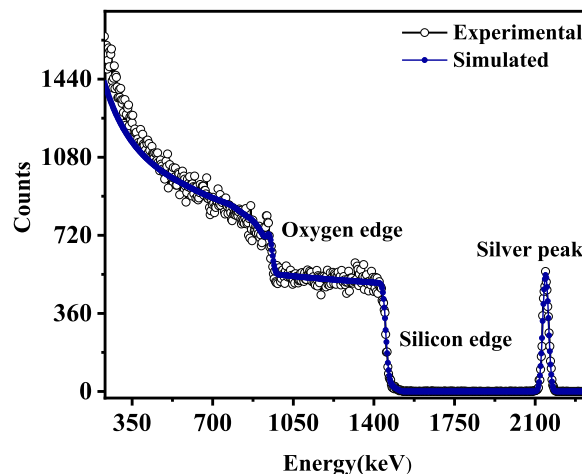


FIG. 2. Experimental and simulated RBS plots for the Ag-Implanted quartz substrate.

Simulation of the experimental spectra gave the thicknesses and elemental composition percentages of the layered microstructure. First layer in the simulation had elemental concentration matching to the chemical composition of quartz substrate. Second layer was simulated with the mixture of Ag, Si and O. A depth scale of 10^{15} atoms/cm² is characteristic of RBS analysis, which describes the number of target atoms visible to the incident ion beam. Using the bulk density of quartz (2.65 g/cm³), thickness of 1st layer was estimated to be at 16 nm. This result suggests that the silver edge in the RBS spectra is at 16 nm below the surface and is in close agreement with SRIM calculations (Fig. 1).

The RBS spectra that show the scattering of Ag for all the implanted substrates are shown in Fig. 3. Increase in peak intensities of Ag peak in the spectra is indicative of the expected increase in concentration of silver at fixed depth below the surface. The SIMNRA simulation of RBS data gave fluences of 0.8×10^{16} p/cm², 1.1×10^{16} p/cm², 1.3×10^{16} p/cm², 1.5×10^{16} p/cm² and 3.0×10^{16} p/cm². It is evident from Fig. 3 that the depth where silver was implanted remained fixed despite the increase in the ion beam fluence. However, the increases in the fluence lead to an increase in the size distribution of Ag NPs that will be presented in the following section.

The optical absorption spectra of 70 keV Ag implanted quartz substrates with different fluences are shown in Fig. 4, and characteristic surface plasmon absorption bands was observed confirming the presence of Ag nanoparticles in the quartz substrate. An increase in the optical intensity of the LSPR peak was observed with increased concentration of the silver ion beam. The increase in the absorption intensity with increasing fluence creates higher density of the Ag atoms in the implanted layer thereby increasing the number of silver nanoparticles that were developed in the quartz but also suggests an increase in the size of nanoparticles. The inset of Fig. 4 shows the normalized LSPR peaks at different ion beam fluence. An increase in the fluence displays broadening as well as red shift of LSPR peak that can be ascribed to increased inter-particle electromagnetic coupling³⁵ as well as to increased size of the Ag nanoparticles.³⁶ The increase in the size of nanoparticles can be ascribed to the enhanced diffusion due to concentration gradients of silver atoms. Diffusion within the matrix could be associated with the localized beam heating during the ion implantation process. Similar behavior was observed in literature.^{37,38} The size of nanoparticles can be calculated from the optical absorption spectra and such analysis is presented below.

The UV/Vis spectra of the nanoparticles were simulated using Mie theory calculations.³³ In the present simulation, a spherical shape was assumed for the nanoparticles and the absorption spectra of silver NPs with diameters from 1 nm to 15 nm were calculated using Mie theory, and then simulated the total absorption spectra from the absorption spectra of different sized nanoparticles using.³⁹

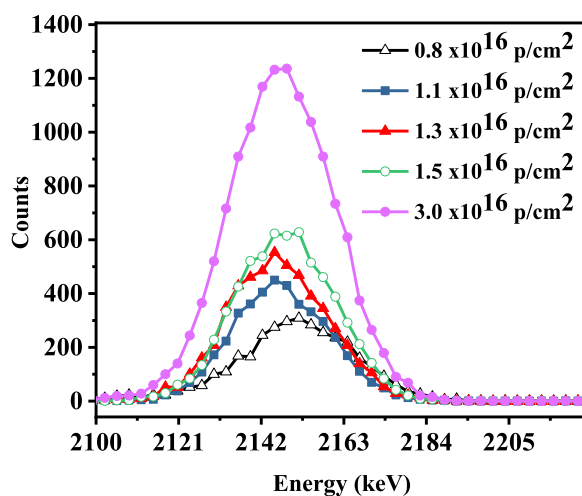


FIG. 3. Overlapped experimental RBS spectra for backscattered He ions between 2100-2226 keV showing the peak intensity increase with fluence for Ag implanted in quartz substrate.

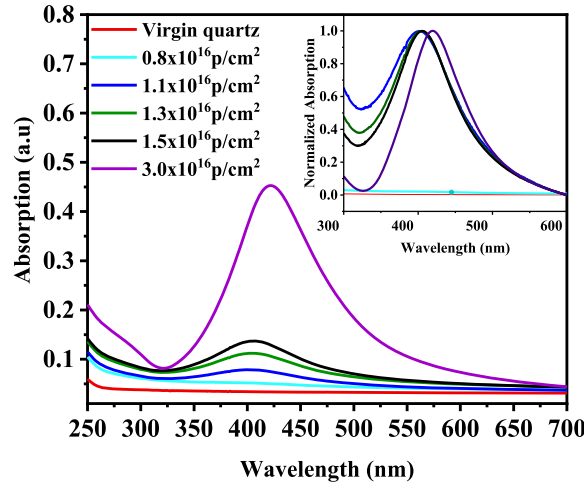


FIG. 4. Absorption spectra of Ag implanted NPs within quartz substrate for different fluences. Absorption intensity increases as Ag ion fluence increases. Inset of the figure is normalized plot, clearly showing red-shift of the LSPR peak with increasing Ag ion fluence.

$$C_{T,abs} = \sum_i W_i C_{abs}(i) \quad (1)$$

where, W_i , and $C_{abs}(i)$ are the weighting factor and the absorption spectra of cluster (i), respectively. With decreasing the size of the NPs, surface scattering increases, resulting an increase in the damping frequency of the NPs due to reducing mean free path of the conduction electrons in the MNPs. To consider this effect on the calculation, modified collision frequency for the small MNPs was used and is given by:

$$\gamma_{Nps} = \gamma_{bulk} + \frac{AV_F}{r} \quad (2)$$

where γ_{bulk} is the collision frequency of the bulk metal ($\hbar\gamma_{bulk} = 0.016$ eV for silver⁴⁰), A is the fitting parameter, V_F is the Fermi velocity ($V_F = 1.4 \times 10^6$ ms⁻¹ in silver⁴¹) and r is radius of the nanoparticles.

Considering aforementioned damping effect, the modified permittivity of the metallic nanoparticles can be expressed as:⁴²

$$\epsilon_{Np}(\omega, r) = \epsilon_{bulk}(\omega) + \frac{\omega_p^2}{\omega^2 + i\gamma_{bulk}\omega} - \frac{\omega_p^2}{\omega^2 + i\gamma_{Nps}\omega} \quad (3)$$

where $\epsilon_{bulk}(\omega)$ is the frequency dependent permittivity of the bulk of silver and ω_p is plasma frequency ($\hbar\omega_p = 9.01$ eV for silver⁴³).

By shrinking the size of nanoparticles below 10 nm the band structure of the MNPs will be discretized. Due to discretization of the conduction band of the NPs, only certain electronic or plasmonic transition are allowed.⁴⁴ In order to accurately simulate the optical properties of these small sized NPs, quantum effects are considered in the present simulation.³⁶ In addition, to calculate total absorption spectra of the samples, corresponding weighting factor (W_i) of each cluster needed to be optimized. Harmony Search Algorithm (HSA) was applied for adjusting the W_i . This algorithm is a music-based algorithm that relies on the search process for optimization and it can be compared to jazz musician's improvisation process.⁴⁵

For the present system, initially an average error between the experimental and the theoretical absorption spectra as objective function was defined. Then, a weighting factor of each cluster, as an optimization parameter, has been chosen randomly between 0 and 1. These parameters are stored in a row vector of X_j as below:

$$X_j = [W_j^1, W_j^2, W_j^3, \dots, W_N^j] \quad (4)$$

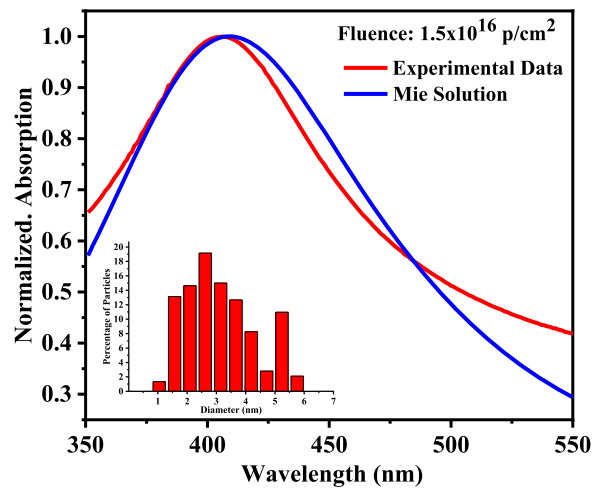


FIG. 5. Comparison of normalized absorption spectra of the experimental and the optimized theoretical data. Corresponding size distribution plot for the Ag-Implanted sample is shown in the inset.

By tuning the optimization parameters of X_j and minimizing the objective function using HSA, average size of the silver nanoparticles in each sample and their corresponding errors were determined. There representative experimental and simulated absorption spectra of the Ag-ion implanted sample at 1.5×10^{16} p/cm² fluence is shown in Fig. 5 and the size distribution is presented in the inset of Fig. 5. There is a good agreement between the experimental and simulated data. Also, a distribution of sizes was needed to fit the experimental data that shows that there is a significant polydispersity with ion beam implantation, which was expected as post implantation annealing was not carried out for this study. It is also evident from the calculations that most of the discrepancies between simulation and experimental spectra were found in the off-resonance wavelengths where slight deviation of the shape of nanoparticles from spherical shape can lead to significant changes. Interestingly, as the ion fluence increases, the average size of the nanoparticles is increased from 2.2 nm to 5.6 nm (Fig. 6). The results are consistent with the fact that at higher ion beams fluences, localized Ag ion concentration gradients increases resulting in increased average size of the nanoparticles.

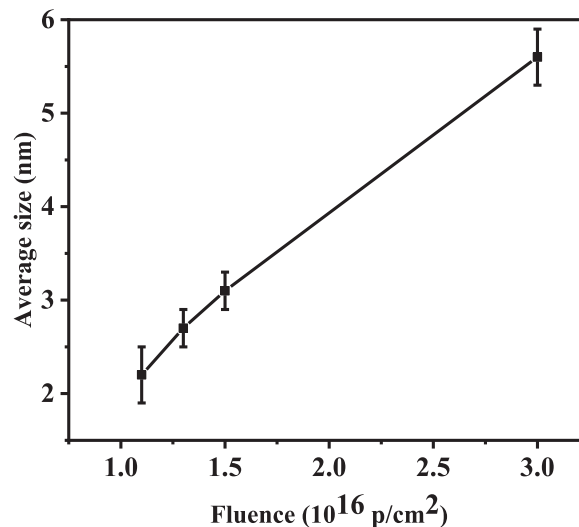


FIG. 6. Theoretical evaluation of the average size of the implanted Ag- NPs in quartz matrix as function of Ag ions fluence determined by Mie-theory calculations.

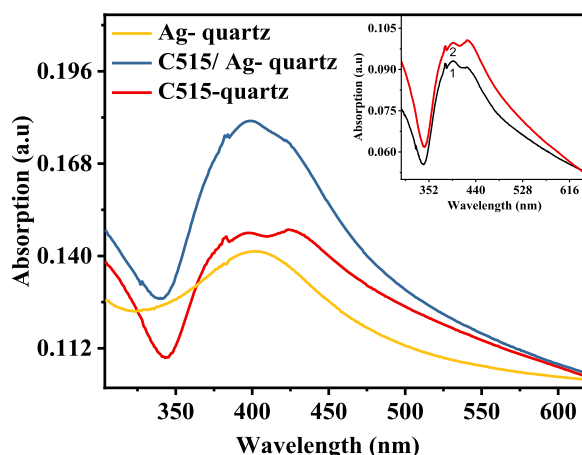


FIG. 7. Optical absorption spectra of Ag-Implanted quartz substrate, C515/Ag-NPs on quartz and C515 on bare quartz. Inset represent (1) Ag-NPs absorption subtracted from drop casted C515 on Ag-Implanted quartz and (2) C515 on bare quartz.

The focus of the present study is to probe the effect of ion implanted Ag-NPs on the fluorescence properties of adsorbed dye. For the investigation, we chose C515 dye as it is photo-stable and its photo-physics is well studied.³⁹ For the measurements, C515 dye was drop-casted on bare and implanted quartz substrates. The optical absorption spectrum of Ag-NPs with and without drop casted C515 is shown in Fig. 7 for a fluence of 1.1×10^{16} p/cm². It can be observed from Fig. 7 that there is an increase in the absorption for the C515 drop casted dye on the ion implanted substrate as compared to the ion implanted substrate without C515 on the surface. The absorption increase is consistent with the mutual addition of the C515 absorption and Ag-NP absorption. To obtain the absorption of C515 in the presence of Ag-NPs, absorption of Ag-NPs was subtracted and presented in the inset of Fig. 7. The absorption of C515 seems to be unaffected with silver nanoparticles indicating that there is no direct ground state interaction between the dye and nanoparticle (inset of Fig. 7). This is an important aspect for using ion implanted Ag-NPs for MEF of dye molecules. It is well known that the fluorescence of dye molecules is often quenched in the presence of MNPs.^{46,47}

Optimized to the dye concentration plot of fluorescence of C515 dye (after excitation at 410 nm), measured on bare and on Ag implanted quartz substrate for different silver ion fluences is shown in Fig. 8. An increase in the fluorescence intensity was observed for C515 in the presence of silver

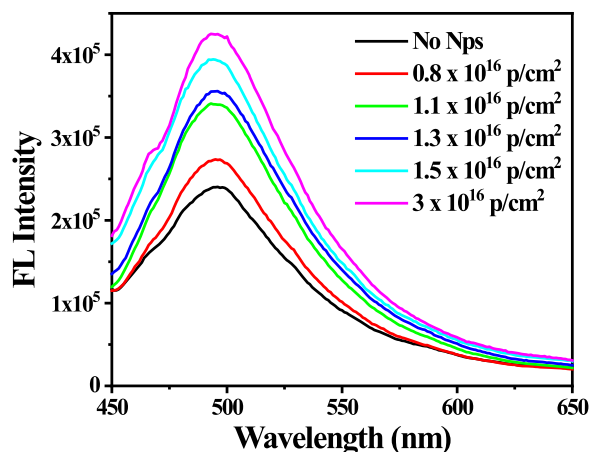


FIG. 8. Fluorescence spectra of C515 dye after excitation at 410 nm in the presence of embedded silver nanoparticles synthesized at different silver ion beam fluences.

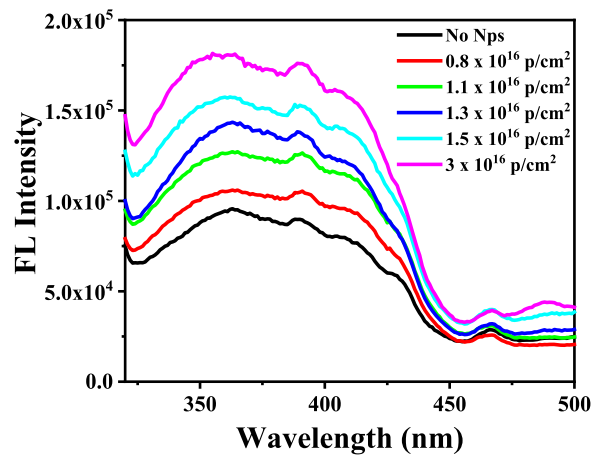


FIG. 9. Excitation spectra of C515 dye on silver-implanted substrates. Note the increase in excitation with the increase in Ag ion fluence.

nanoparticles indicating the influence of MEF. In addition, as demonstrated clearly in Fig. 8, the fluorescence intensity of C515 in the presence of the Ag-NPs is enhanced by increasing the fluence of Ag ions. Interesting aspect of the fluorescence enhancement is the fact that the 350 nm excitation lead to greater increase when compared to 450 nm excitation. To quantify this effect, excitation spectra were measured while monitoring the fluorescence at 510 nm. An excitation spectrum after optimizing to the concentration of the dyes is presented in Fig. 9. For C515-quartz, the excitation spectra resemble the C515 in solution. However, with increase in Ag-NPs fluence, the higher energy side of the excitation spectra has shown a significant increase. This result suggests the influence of silver nanoparticle on the fluorescence enhancement of C515. For further analysis, the ratio of excitation intensities at 350 nm to 450 nm was determined for all substrates and is provided in Fig. 10. Note from the figure that the ratio on bare quartz is around 4, but it increased to 9 at highest Ag-NPs concentration, which confirms that MEF is quite prominent with ion implanted Ag-NPs. Corresponding enhancement factor as a function of Ag-ion beam fluence and the size of the nanoparticles is provided in Table I. The PL enhancement factor was determined from the ratio of excitation intensities with and without Ag-NPs.

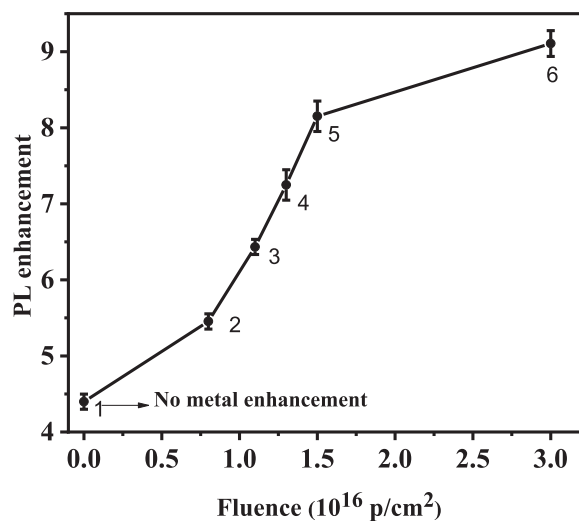


FIG. 10. Photoluminescence enhancement for (1) bare quartz, (2) 0.8×10^{16} p/cm², (3) 1.1×10^{16} p/cm², (4) 1.3×10^{16} p/cm², (5) 1.5×10^{16} p/cm², and (6) 3.0×10^{16} p/cm² Ag ion implanted quartz.

TABLE I. PL enhancement determined from excitation intensity ratio at 350 nm to 450 nm for C515/Ag-NPs and normalized with bare quartz PL excitation intensity ratio.

Fluence (p/cm^2)	Average size (nm)	PL enhancement factor
0.8×10^{16}	-	1.2 ± 0.1
1.1×10^{16}	2.2 ± 0.3	1.5 ± 0.1
1.3×10^{16}	2.7 ± 0.2	1.7 ± 0.2
1.5×10^{16}	4.4 ± 0.2	1.9 ± 0.2
3.0×10^{16}	5.6 ± 0.3	2.1 ± 0.2

The results provided in Table I shows that close to 2.1 ± 0.2 PL enhancement factor was observed at highest silver nanoparticle concentration that can be entirely ascribed to MEF. In addition, fluorescence lifetimes of C515 were also monitored using time-correlated single photon counting for all samples (Fig. 11). Two exponential decay functions were used to fit the data and an average fluorescence lifetime was determined from the fitting, as shown in inset of Fig. 11. The average lifetimes for C515/quartz was determined to be around 4.1 ± 0.5 ns and it remained unchanged for all the ion implanted substrates suggesting that the silver nanoparticles do not quench the fluorescence of the adsorbed fluorophore. This phenomenon is probably due to enough separation distance between Ag-NPs and C515 dye that do not alter radiative decay of excited C515. Then, what is the reason why such MEF was observed for these systems? It can be explained as follows.

The PL enhancement of C515 is due to the LSPR of Ag-NPs and plasmonic hot spots. The interaction of light with the conduction-band electrons on the surface of MNPs generate strong localized electric field around silver NPs. This increases the excitation field around molecule which leads to enhanced absorption of light. This field does not affect the lifetime of excited state of fluorophore.⁴ Our results support that the fluorescence enhancement of fluorophore is stronger around larger size MNPs that enhances plasmonic mode, resulting in strong fluorescence enhancement. In addition, by increasing the fluence of Ag-NPs, dimension of the particles in matrix increases and the inter-particles distance decreases, resulting in creation of plasmonic hot spots between the neighboring particles and consequently several fold enhancement of the electric field between them in comparison to non-interacting NPs.^{14,15} Such hot spots with enhanced plasmonic fields is primary mechanism for SERS that can amplify the fluorescence of fluorophores. The overall mechanism of MEF observed in the present system can be ascribed to increased particle sizes and their magnified LSPR effect and to increased concentration of silver nanoparticles leading to amplified plasmonic hot spots that in turn leads to enhanced fluorescence of fluorophore.

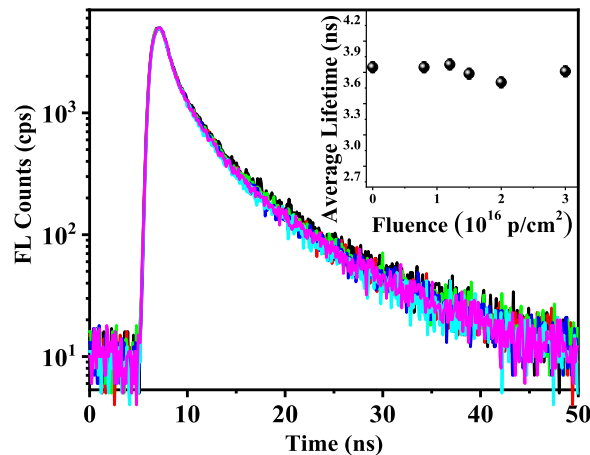
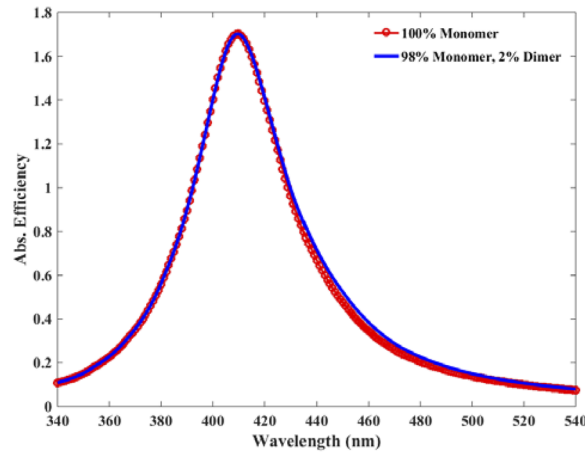
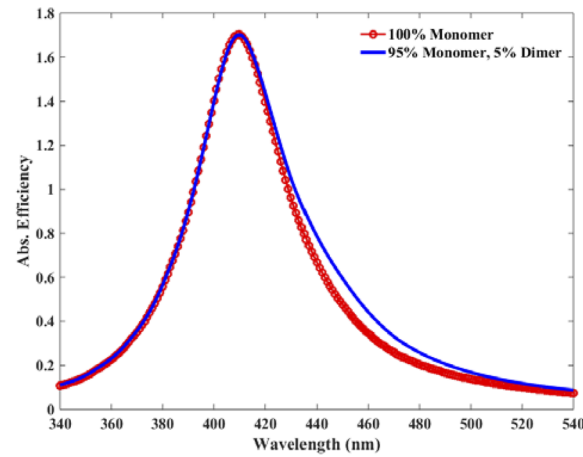


FIG. 11. Time resolved fluorescence of C515 at different ion-implanted silver nanoparticle substrates. Inset shows the average lifetime of C515.



(a)



(b)

FIG. 12. Absorption efficiency of Ag-NPs with diameter of 5.6 nm inserted a quartz medium with weight factors of: (a) $W_{\text{dimer}} = 0.02$, $W_{\text{monomer}} = 0.98$, (b) $W_{\text{dimer}} = 0.05$, $W_{\text{monomer}} = 0.95$.

In our simulation, we did not consider the LSPR coupling effect for calculating the absorption and scattering spectra of the MNPs. It was assumed that the influence of LSPR coupling has smaller effect on the absorption and scattering of the nanoparticles while it has significant effect on enhancing the fluorescence of dye molecules via electromagnetic field enhancement. As an example, we calculated absorption spectra of single Ag-NPs with diameter of 5.6 nm embedded in quartz (Fig. 12). To obtain influence of the dimer of NPs on the absorption spectra, absorption cross section of sample has been simulated using Discrete Dipole Approximation^{48,49} (DDA) for two different weight factors: 1) $W_{\text{dimer}} = 0.02$, $W_{\text{monomer}} = 0.98$, 2) $W_{\text{dimer}} = 0.05$, $W_{\text{monomer}} = 0.95$. In our simulation, surface - surface inter-particle distance was set to 1 nm and incident electric field was oriented in the direction of the inter-particle axis. As clearly can be understood from these figures, LSPR coupling has negligible influence on the absorption spectra of the NPs. However, coupling between neighboring particles produces strong electric field between two MNPs which is more than three times stronger than single one (see Fig. 13). This coupling effect leads to 100 times stronger fluorescence enhancement than single MNPs.

Ion-implanted silver nanoparticles inside quartz matrix were synthesized, characterized and used to achieve MEF. A low energy silver ion beam of different fluences with fixed energy of 70 keV

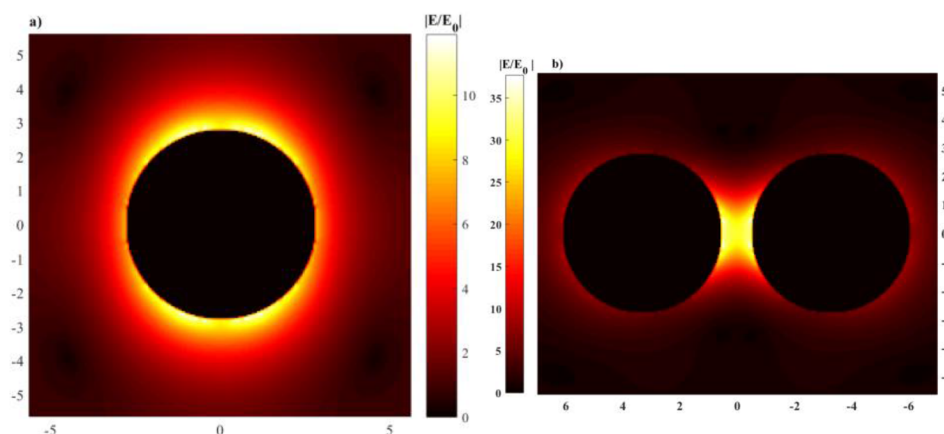


FIG. 13. Plasmonic field enhancement due to hot spots for the spherical NPs with diameter of the 5.6 nm: a) Monomer, b) Dimer.

was used to fabricate silver nanoparticles inside quartz matrices. Optical absorption spectrum of implanted samples confirmed the formation of the silver NPs within the quartz matrix. By comparing experimental absorption and theoretical cross section (using Mie theory) of the samples, we were able to show that the nanoparticle size increases with an increase in the ion beam fluence. RBS measurements corroborated SRIM calculations that the silver nanoparticles were formed at a depth of 16 nm from the surface. MEF measurements were carried out with C515 dye drop casted on the quartz surface and fluorescence enhancement was observed. The enhancement factor was estimated from the excitation ratio of 350 nm to 450 nm where the silver nanoparticle dominates the higher energy absorption. From our measurements, close to 2.1 ± 0.2 enhancement factor was observed at highest ion beam fluence. The observed MEF was attributed to plasmon enhancement with large sized nanoparticles as well as the presence of hot spots between silver NPs. This new approach provides quartz matrices embedded with metal nanoparticle that can be used as substrates for plasmon sensing as well as biological imaging.

- ¹ E. J. Blackie, E. C. Le Ru, and P. G. Etchegoin, *Journal of the American Chemical Society* **131**, 14466 (2009).
- ² D.-K. Lim, K.-S. Jeon, H. M. Kim, J.-M. Nam, and Y. D. Suh, *Nature Materials* **9**, 60 (2010).
- ³ Y. A. Krutyakov, A. A. Kudrinskiy, A. Y. Olenin, and G. V. Lisichkin, *Russian Chemical Reviews* **77**, 233 (2008).
- ⁴ W. Deng, F. Xie, H. T. M. C. M. Baltar, and E. M. Goldys, *Physical Chemistry Chemical Physics : PCCP* **15**, 15695 (2013).
- ⁵ D. Darvill, A. Centeno, and F. Xie, *Physical Chemistry Chemical Physics* **15**, 15709 (2013).
- ⁶ K. Aslan, M. J. R. Previte, Y. Zhang, and C. D. Geddes, *Analytical Chemistry* **80**, 7304 (2008).
- ⁷ F. Tam, G. P. Goodrich, B. R. Johnson, and N. J. Halas, *Nano Letters* **7**, 496 (2007).
- ⁸ A. S. Thakor and S. S. Gambhir, *CA: A Cancer Journal for Clinicians* **63**, 395 (2013).
- ⁹ L. Duchesne and D. G. Fernig, *Analytical Biochemistry* **362**(2), 287–289 (2007).
- ¹⁰ J. Vuckovic, M. Loncar, and A. Scherer, *IEEE Journal of Quantum Electronics* **36**, 1131 (2000).
- ¹¹ O. Painter, *Science* **284**, 1819 (1999).
- ¹² C. D. Geddes, H. Cao, I. Gryczynski, Z. Gryczynski, J. Fang, and J. R. Lakowicz, *Journal of Physical Chemistry A* **107**, 3443 (2003).
- ¹³ A. S. Kumbhar, M. K. Kinnan, and G. Chumanov, *Journal of the American Chemical Society* **127**, 12444 (2005).
- ¹⁴ A. Bek, R. Jansen, M. Ringler, S. Mayilo, T. A. Klar, and J. Feldmann, *Nano Letters* **8**, 485 (2008).
- ¹⁵ S. T. Kochuveedu and D. H. Kim, *Surface Plasmon Enhanced, Coupled and Controlled Fluorescence* (2017), pp. 179–195.
- ¹⁶ J. Zang, Y. Fu, D. Liang, R. Y. Zhao, and J. R. Lakowicz, *Langmuir* **24**, 12452 (2008).
- ¹⁷ J. Zhang, Y. Fu, M. H. Chowdhury, and J. R. Lakowicz, *Nano Letters* **7**, 2101 (2007).
- ¹⁸ K. Aslan, J. R. Lakowicz, and C. D. Geddes, *Journal of Physical Chemistry B* **109**, 6247 (2005).
- ¹⁹ K. Aslan, Z. Leonenko, J. R. Lakowicz, and C. D. Geddes, *The Journal of Physical Chemistry. B* **109**, 3157 (2005).
- ²⁰ D. Wakuda, K. S. Kim, and K. Suganuma, *Scripta Materialia* **59**, 649 (2008).
- ²¹ C. D. Geddes, *Surface Plasmon Enhanced, Coupled and Controlled Fluorescence* (2016).
- ²² A. Meldrum, L. Boatner, and C. White, *Nuclear Instruments and Methods in Physics Research Section B: Beam Interactions with Materials and Atoms* **178**, 7 (2001).
- ²³ F. Ren, X. H. Xiao, G. X. Cai, J. B. Wang, and C. Z. Jiang, *Applied Physics A: Materials Science and Processing* **96**, 317 (2009).
- ²⁴ O. P. R. Pal, Umapada (2012).
- ²⁵ P. Benzo, L. Cattaneo, C. Farcau, A. Andreozzi, M. Perego, G. Benassayag, B. Pécassou, R. Carles, and C. Bonafos, *Journal of Applied Physics* (2011).

- ²⁶ P. Benzo, C. Bonafos, M. Bayle, R. Carles, L. Cattaneo, C. Farcau, G. Benassayag, B. Pécassou, and D. Muller, *Journal of Applied Physics* (2013).
- ²⁷ M. Bayle, C. Bonafos, P. Benzo, G. Benassayag, B. Pécassou, L. Khomenkova, F. Gourbilleau, and R. Carles, *Applied Physics Letters* (2015).
- ²⁸ C. Farcau, C. Bonafos, P. Benzo, G. Benassayag, and R. Carles, *Journal of Applied Physics* (2010).
- ²⁹ A. L. Stepanov and V. N. Popok, *Surface and Coatings Technology* (2004).
- ³⁰ A. L. Stepanov, D. E. Hole, and P. D. Townsend, *Nuclear Instruments and Methods in Physics Research Section B: Beam Interactions with Materials and Atoms* (1999).
- ³¹ A. L. Stepanov, *Rev. Adv. Mater. Sci* (2011).
- ³² J. F. Ziegler, M. D. Ziegler, and J. P. Biersack, *Nuclear Instruments and Methods in Physics Research, Section B: Beam Interactions with Materials and Atoms* **268**, 1818 (2010).
- ³³ G. Mie **25**, 377 (1908).
- ³⁴ M. Mayer, Report IPP 9/113 (1997).
- ³⁵ W. Rechberger, A. Hohenau, A. Leitner, J. R. Krenn, B. Lamprecht, and F. R. Aussenegg, *Optics Communications* (2003).
- ³⁶ L. M. Liz-Marzán, *Langmuir* **22**, 32 (2006).
- ³⁷ L. C. Nistor, J. van Landuyt, J. D. Barton, D. E. Hole, N. D. Skelland, and P. D. Townsend, *Journal of Non-Crystalline Solids* **162**, 217 (1993).
- ³⁸ A. A. Bukharaev, V. M. Janduganov, E. A. Samarsky, and N. V. Berdunov, *Applied Surface Science* **103**, 49 (1996).
- ³⁹ N. Felidj, J. Aubard, and G. Levi, *The Journal of Chemical Physics* **111**, 1195 (1999).
- ⁴⁰ L. Genzel, T. P. Martin, and U. Kreibig, *Z. Phys. B-Condens. Mat.* **21**, 339 (1975).
- ⁴¹ U. Kreibig and C. V. Fragstein, *Zeitschrift für Physik* **224**, 307 (1969).
- ⁴² J. Romann, J. Wei, and M. P. Pileni, *Journal of Physical Chemistry C* **119**, 11094 (2015).
- ⁴³ A. D. Rakić, A. B. Djurišić, J. M. Elazar, and M. L. Majewski, *Applied Optics* **37**, 5271 (1998).
- ⁴⁴ J. A. Scholl, A. L. Koh, and J. A. Dionne, *Nature* **483**, 421 (2012).
- ⁴⁵ M. Mahdavi, M. Fesanghary, and E. Damangir, *Applied Mathematics and Computation* **188**, 1567 (2007).
- ⁴⁶ E. Dulkeith, A. C. Morteani, T. Niedereichholz, T. A. Klar, J. Feldmann, S. A. Levi, F. C. J. M. van Veggel, D. N. Reinhoudt, M. Möller, and D. I. Gittins, *Physical Review Letters* **89**, 203002 (2002).
- ⁴⁷ N. S. Basheer, B. R. Kumar, A. Kurian, and S. D. George, *Journal of Luminescence* **137**, 225 (2013).
- ⁴⁸ B. T. Draine and P. J. Flatau, *Journal of the Optical Society of America A* (1994).
- ⁴⁹ J. Mc Donald, A. Golden, and S. G. Jennings, *International Journal of High Performance Computing Applications* (2009).